Response to reviewers - Rethinking fractal scaling of sea ice deformation: the dominant role of signed-gradient cancellation

Florence L. Beaudry and L. Bruno Tremblay

October 26, 2026

Legend

Original Comments
Responses
Changes to the manuscript

Reviewer #2

Review for "Rethinking fractal scaling of sea ice deformation: the dominant role of signed-gradient cancellation"
by Beaudry & Tremblay

Scaling analyses are a common tool in the sea ice modelling community to quantify and evaluate small-scale sea-ice deformation. Here, power-law scaling of the mean total deformation rate is interpreted as a proof that deformation rates are scale invariant and strongly localized, with the scaling exponent providing information on the degree of localization. The validity of this interpretation has been discussed in the sea ice community more regularly in the past years, for instance in the SIREx model intercomparison project that highlighted the ambiguity of the metric. Using synthetic sea ice velocity data, this manuscript illustrates that neither localized deformation necessarily leads to scaling nor scaling behavior is sufficient proof for localized deformation fields. The authors offer a plausible reasoning that the cancellation of signed velocity gradients yields mainly drives the total deformation rates computed by at different length scales and thereby scaling. In

a suite of different tests, the authors outline the shortcomings of scaling analyses. The presented analysis is sound and follows community standards, however descriptions and discussions need further clarification before publication. As outlined above, the presented manuscript clearly addresses main open points in the discussion of how or even if to use scaling analysis in model evaluation at all and I, therefore, suggest to further guide this manuscript to publication. In the following, I outline my major and specific comments that should be considered before publication.

We thank the reviewer for the thorough review and useful suggestions on the manuscript.

Major comments:

1. Scaling method: The paper uses and discusses only coarse-graining as a method to compute spatial scaling. However, also triangulation approaches using line integral computations of deformation rates are a common method to compute deformation rates at different scales (e.g. Hutchings et al., 2011; Oikkonen et al., 2017; Hutchings et al. 2024). While I do not think that the same set of experiments should also be repeated with the triangulation method, the authors should discuss how their findings relate or apply to this method. Do the same conclusions hold up? The triangulation approach may also allow for repeated random sampling to compensate for instance the invariance under rotation.

Our conclusions apply to triangulation approaches as well; in these methods, deformation rates over a polygon P (commonly a triangle) are computed from line integrals of velocity along its boundary. For the axial term with K corners ordered counterclockwise (index $K+1=1$),

$$\left.\frac{\partial u}{\partial x}\right|_P = \frac{1}{A_P}\oint_{\partial P} u\,dy = \frac{1}{2A_P}\sum_{i=1}^{K}(u_i + u_{i+1})(y_{i+1} - y_i). \tag{1}$$

By the divergence theorem, as pointed out by Reviewer #1, this is equivalent to averaging the signed velocity gradients with the polygon, so opposite-sign gradients enclosed by a large polygon cancel in the same way as within a coarse-graining box.

This can be shown with the same idealized fields as in Eqs. 10-12 of the manuscript; one-grid-cell-wide LKFs spaced s grid cells apart, with $u = u(x)$ and each LKF producing a velocity jump $\Delta u_m = \dot{\varepsilon}_0 \Delta x/\sqrt{2}$ (so that $\dot{\varepsilon}_{tot} = \sqrt{2}|\partial u/\partial x| = \dot{\varepsilon}_0$ on each LKF). For any polygon with $u = u(x)$, the sum above reduces to the velocity differences across it, so that $\dot{\varepsilon}_{tot} = \sqrt{2}|u(x_R) - u(x_L)|/L$, where x_L and x_R are its left and right edges and L its width. At the smallest scale, each grid cell ($K = 4, A = \Delta x^2$) contains at most one LKF, and the line integral of these non-zeros cells reduces to the finite difference of Eq. 6 of the

manuscript:

$$\langle \dot{\varepsilon}_{tot} \rangle_{L=\Delta x} = \frac{1}{N_x^2} \sum_{i}^{N_x^2/s} \frac{\sqrt{2}}{\Delta x} |u(x_i + \Delta x) - u(x_i)| = \frac{\dot{\varepsilon}_0}{s}. \tag{2}$$

At the largest scale, the polygon is the whole domain ($A = N^2$, with $N = N_x \Delta x$), and only the boundary velocities contribute:

$$\langle \dot{\varepsilon}_{tot} \rangle_{L=N} = \frac{\sqrt{2}}{N} |u(N) - u(0)| = \frac{\sqrt{2}}{N} \left| \sum_{m=1}^{N_x/s} \Delta u_m \right| = \begin{cases} \dot{\varepsilon}_0/s & \text{if same-sign LKFs,} \\ 0 & \text{if alternating-sign LKFs.} \end{cases} \tag{3}$$

As with coarse-graining (Eqs. 10–12 of the manuscript), same-sign LKFs give identical mean total deformation at the smallest and largest scales ($\beta = 0$), whereas alternating-sign LKFs cancel in the velocity difference across the domain, producing scale dependence. The same result is obtained with triangles ($K = 3$), since the line integral depends only on the velocities at the polygon boundary. We also agree that triangulation approaches may have an advantage regarding rotation. We have added the following to the Conclusions (after L349):

We present coarse-graining in this study. Deformation rates at different scales are also commonly computed from line integrals of velocity around polygons, often triangles, of increasing size defined by buoy arrays or Lagrangian tracking (e.g., Hutchings et al., 2011; Oikkonen et al., 2017; Hutchings et al., 2024). By the divergence theorem, these line integrals are equivalent to averaging the signed velocity gradients within each polygon, so that the same signed-gradient cancellation mechanism controls the scale dependence in the Lagrangian method. The different shapes and orientations of these polygons, and the possibility of random resampling, would however likely reduce the non invariance under rotation described in Sec. 3.4.

2. C-grid discretization: The computation of deformation rates in this manuscript is based on a C-grid discretization, where the off-diagonal elements of the deformation matrix are computed over a larger stencil than the on-diagonal elements. This discretization choice should be discussed in more detail and compared to other choices, since it is not the same as other scaling papers used, e.g. SIREx.

We used the C-grid stencil because it is the discretization of choice in many sea ice models (e.g., MITgcm, Losch et al., 2010; SI3, Vancoppenolle et al., 2023; SIS2, Adcroft et al., 2019); the synthetic experiments therefore mirror how the diagnostic is applied to model output on native grids. The location of the velocity vector on the C-grid is more natural for the discretization of the advection equation for mass and concentration, is more direct for coupling with C-grid ocean and atmospheric models, and better represents inertial–plastic

compressive waves (Bouillon et al., 2009). For these reasons, members of the CICE Consortium decided to implement a finite-difference C-grid capability in CICE (Lemieux et al., 2024), whose discretization we follow here.

The discretization differs from the approach used in SIREx, where velocity gradients were computed from line integrals around Lagrangian cells for both RGPS and models (Bouchat et al., 2022b). Moreover, the conclusions presented in the manuscript are robust to the choice of stencil. In the experiments of Secs. 3.1-3.3, only diagonal terms, which are identical in both B- and C- grid, are used. In the rotation experiment presented in Sec. 3.4, off-diagonal terms associated with shear are present, and while the B-grid discretization differs from that of the C-grid, the results are nearly identical (Figs. R1–R2).

Finally, the analyses of RGPS and SIREx deformations presented in Secs. 3.5–3.7 are computed directly from line integrals of velocity and do not depend on the choice of stencil. We have revised Sec. 2.3 (L160) to clarify this point:

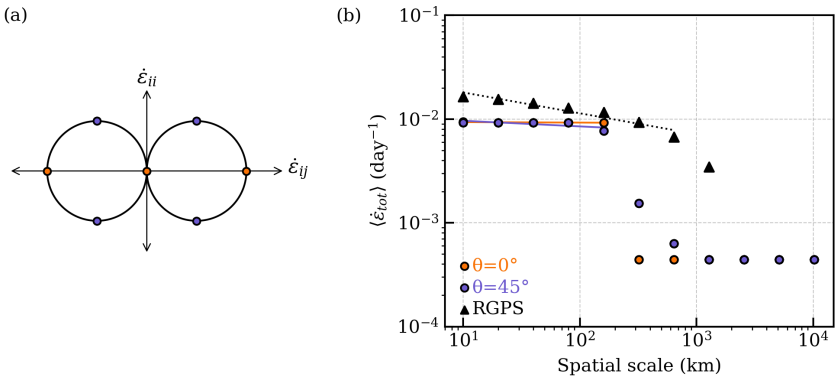


Figure R1: B grid

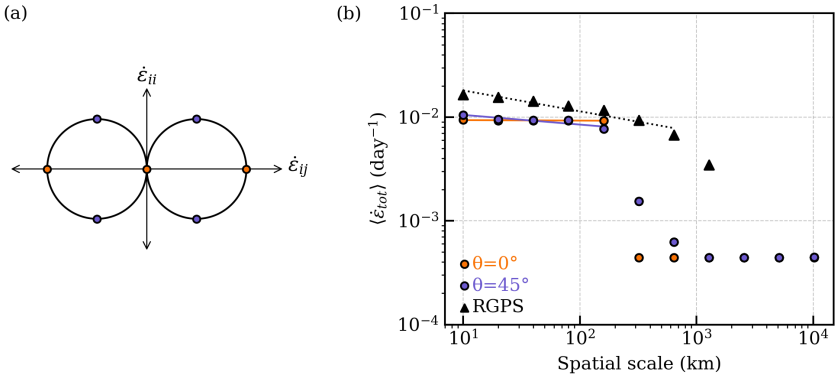


Figure R2: C grid; New Fig. 4

We use the C-grid stencil because it is the discretization of choice in many sea ice mod-

els (e.g., MITgcm, Losch et al. 2010; SI3, Vancoppenolle et al. 2023; SIS2, Adcroft et al. 2019); the synthetic experiments therefore mirror how the diagnostic is applied to model output on native grids. Note that the choice of stencil only affects the off-diagonal (shear) terms; the diagonal terms used in Sections 3.1–3.3 are identical on the B- and C-grids. Repeating the rotation experiment of Section 3.4 on an Arakawa B-grid, where all four gradients share the same stencil, yields nearly identical results (not shown). The RGPS and SIREx deformation rates analyzed in Sections 3.5–3.7 are computed using a line-integral approach (Bouchat et al., 2022b) and are therefore independent of the stencil choice.

3. Scaling of higher moments: The authors focus on first-order (spatial) scaling properties in the presented manuscript. Scaling analyses of higher moments use the same principle to compute deformation rates at different scales and are used to quantify the multi-fractality of sea-ice deformation. Despite the methodological similarities, an in-depth discussion or outlook what the presented findings might imply for these multi-fractal analyses are missing the manuscript.

We added a paragraph in the Conclusions discussion regarding the extension of this work to higher moment of the total deformation distribution at L349. Higher-order structure functions are computed from the same coarse-grained signed gradients, so signed-gradient cancellation enters before the moments are taken. Since our results show that the first-order exponent cannot be interpreted as a measure of localization, the dependence of the higher-order exponents on moment order cannot be interpreted as such either, at least as these diagnostics are currently used.

Our analysis focused on first-order spatial scaling, but the same limitation extends to higher-order moments. Multifractal analyses characterize how the scaling exponent $\beta(q)$ of the moments $\langle \dot{\varepsilon}_{tot}^{q} \rangle_L \propto L^{-\beta(q)}$ varies with the moment order q, and interpret the curvature of $\beta(q)$ as a measure of localization and intermittency (e.g., Marsan et al., 2004; Rampal et al., 2019; Uusinoka et al., 2025b). These moments are computed from the same coarse-grained signed gradients and are therefore subject to the same signed-gradient cancellation. Since the first-order exponent does not measure localization, the dependence of $\beta(q)$ on q cannot be interpreted as such either. Higher-order moments may carry information on the cancellation itself, but this remains to be demonstrated. Until then, they do not provide a more robust basis for model evaluation than β, and the PDF-based diagnostics recommended above remain more directly interpretable.

Specific comments:

L.29-32: "power-law distributions of floe size and deformation, box-counting analyses of SAR backscatter, power spectra of buoy dispersion, and structure functions of mean total strain rates (e.g., Rothrock and Thorndike 1984; Martin and Thorndike 1985; Weiss 2001a, b; Weiss and Marsan 2004; Marsan et al. 2004; Hutchings et al. 2011)."" -> Please move the citations to the different referenced properties.
Corrected as suggested; L28-32 now reads:
Evidence of scale invariance in sea ice deformation, fracture, and fragmentation emerges through multiple avenues, including power-law distributions of floe size (Rothrock and Thorndike, 1984), dispersion of buoys (Martin and Thorndike, 1985), fracture and fragmentation patterns (Weiss, 2001a, b), and structure functions of mean total strain rates (Marsan et al., 2004; Weiss and Marsan, 2004; Hutchings et al., 2011).

L.83: "radarsat" -> capitalize
Corrected as suggested.

L.106: "current practice in the sea ice deformation community" -> There is also an alternative Lagrangian approach, where triangles of different edge length are triangulated from Lagrangian positions and deformation rates are computed from line integrals (e.g. Oikkonen et al., 2017).
We clarified that it is common practice in the community for model evaluation specifically (L106) and acknowledge that the deformation can also be calculated using line integrals around triangular or quadrilateral elements in the Conclusions (see our response to major comment 1).
Following Marsan et al. (2004) and current practice for sea ice model evaluation in the community, we calculate [...]

L.129-130: "Theoretically, when this relationship is log-linear over at least two orders of magnitude, it is referred to as scaling and characterized by the scaling exponent β" -> Is there a citation for this statement?
This criterion was introduced by Hamburger et al. (1996) in the field of physics; no such threshold has been established in the sea ice literature. We have added this reference to the revised manuscript (L129-130).
Theoretically, when this relationship is log-linear over at least two orders of magnitude (Hamburger et al., 1996), it is referred to as scaling and characterized by the scaling exponent β.

L.181: "and/or shear" -> Are you talking about shear as off-diagonal velocity gradients

(du/dy and dv/dx) or the strain invariant eps II? Please clarify, as the latter is positive definite and would not cancel out when average over larger scales.
This sentence refers to the off-diagonal velocity gradients. This has been corrected on L181 in the revised manuscript:
L181: When bands of on-diagonal and off-diagonal velocity gradients of alternating sign are introduced along the same LKFs ($\dot{\varepsilon}_I = (-1)^k \dot{\varepsilon}_0$ for integer k; Fig. 3c), scale dependence emerges.

L.213-214: "the same conclusions hold for experiments with shear deformation, as the signed-gradient cancellation mechanism remains unchanged." -> This needs clarification, as the strain invariant shear cannot have changing signs.
This is clarified in the revised version as suggestion; L213-214 now reads:
L213-214: Note that these experiments are based on synthetic LKFs with divergence only ($\dot{\varepsilon}_I$; $\dot{\varepsilon}_{II} = 0$); the same conclusions hold for experiments with signed off-diagonal (shear) velocity gradients. Although $\dot{\varepsilon}_{II}$ is positive-definite, it is computed from the coarse-grained signed gradients, so cancellation occurs before the invariant is formed.

L.227-228: "since simulated and observed sea ice deformation are computed on different grids" -> That strongly depends on how the comparison is set up. In SIREx for instance the same grid is used. Please clarify.
The deformation in SIREx use the Lagrangian tracking method, but some studies use Eulerian deformation products computed on different grids. This has been clarified in the revised manuscript (L227-228):
L227-228: The non-invariance under rotation could, in principle, have consequences for model evaluation since simulated and observed sea ice deformation are sometimes computed on different grids (Eulerian; e.g., Girard et al. 2011; Bouchat and Tremblay, 2017).

L.230: "rotate velocity gradients in RGPS" -> How do you rotate velocity gradients? Do you rotate the velocities to a different reference frame and then compute the gradients? Please clarify.
The gradient tensor is being rotated, which is equivalent to rotating the velocities; the caption of Fig. 5 has been revised:
Scale dependence of RGPS (normalized) mean total strain rates for 29–31 January 2002, rotated by angle θ. The velocity gradient tensor is rotated as $\nabla \mathbf{u}' = \mathbf{R}(\theta) \nabla \mathbf{u} \mathbf{R}^T(\theta)$, where $\mathbf{R}$ is the 2D rotation matrix, and resampled onto a regular grid of the same spacing via nearest-neighbour interpolation. This is equivalent to expressing the deformation field in a rotated coordinate system, leaving rotational invariants (divergence, maximum shear)

unchanged.

L.265-266: "In contrast, the separation between the cloud of observed and simulated ... (Fig. 7c)." -> It took me some time to understand what you mean here. Please consider explaining this in more detail. Also, if I understood correct the reasoning is that the PDF of <eps tot> dx is different for models and RGPS, whereas the PDF of <eps tot> N is similar for both. This could be easily visualized, when you provide the PDFs in Fig. 7b/c for both RGPS and models at the top of each sub panel.

The reviewer's reading is correct: models and RGPS differ mainly in $\langle \dot{\varepsilon}_{tot} \rangle_{\Delta x}$ (the mean gradient magnitude), whereas $\langle \dot{\varepsilon}_{tot} \rangle_N$ (set by the means of the signed gradients) is similar for all models except FESOM. We clarified this on L265–268 and now refer to Fig. 8, which shows the full gradient PDFs, rather than adding the velocity gradient PDFs to Fig. 7, as suggested by the reviewer.

In contrast, the separation between the cloud of observed and simulated $\tilde{\beta}$ (and β; Fig. 7a) is due to differences in deformation magnitude $\langle \dot{\varepsilon}_{tot} \rangle_{\Delta x}$ (Fig. 7b), rather than in the mean $\langle \dot{\varepsilon}_{tot} \rangle_N$ (Fig. 7c), which falls within the inter-annual variability of RGPS for all models except FESOM. This is consistent with RGPS gradient distributions having heavier tails than those of sea ice models (Fig. 8, left column)

L.288-302: "3.6 Break of scaling at large scale" -> You should test this hypothesis with the SIREx models as well. Depending on the resolution of the model used, the number of LKFs resolved varies significantly and with it also the spacing between them. If your argument holds, models with fewer LKFs should also show a truncation at larger scales. Although, I like the simplicity of your approach of reducing the RGPS domain, it neglects the effect of coastlines in shaping the deformation field, which the model comparison would still include.

We agree with the reviewer that this would be a useful test, but we expect the link between model resolution and the break scale to be indirect. Lower-resolution models resolve fewer LKFs, but these are also wider and more diffuse (Bouchat et al., 2022b, Figs. 9–10), so the spacing and the width of opposite-sign regions change together. SIREx also excludes data within 100 km of the coast, which limits what this comparison could reveal about coastline effects. We therefore leave this to future work and have raised this caveat on L300-302:

Note that our domain reduction experiment is performed independently of LKF positions and therefore may not resample the field in a statistically controlled way. A detailed analysis, including a thorough analysis of how LKF spacing and associated model resolutions impact the scaling and the interactions with coastlines, is beyond the scope of this study.

L.294-295: "To test this hypothesis, we progressively reduced the RGPS domain by a factor of 2 and 4, with respect to the domain centroid." -> Please clarify what exactly you do? Do you mask parts of the RGPS data, do you shrink the data? From the following I assume that you just apply a sequence of decreasing masks to the original data. It might help to include a small sketch as a sub plot in Fig. 10.

The interpretation is correct: we do not shrink or regrid the data, but restrict the analysis to progressively smaller nested square sub-domains centred on the RGPS grid centre, which is equivalent to masking all data outside each sub-domain so the grid spacing is unchanged. We have added a sketch of the sub-domains to Fig. 10, as suggested by the reviewer.

See Fig. R3.

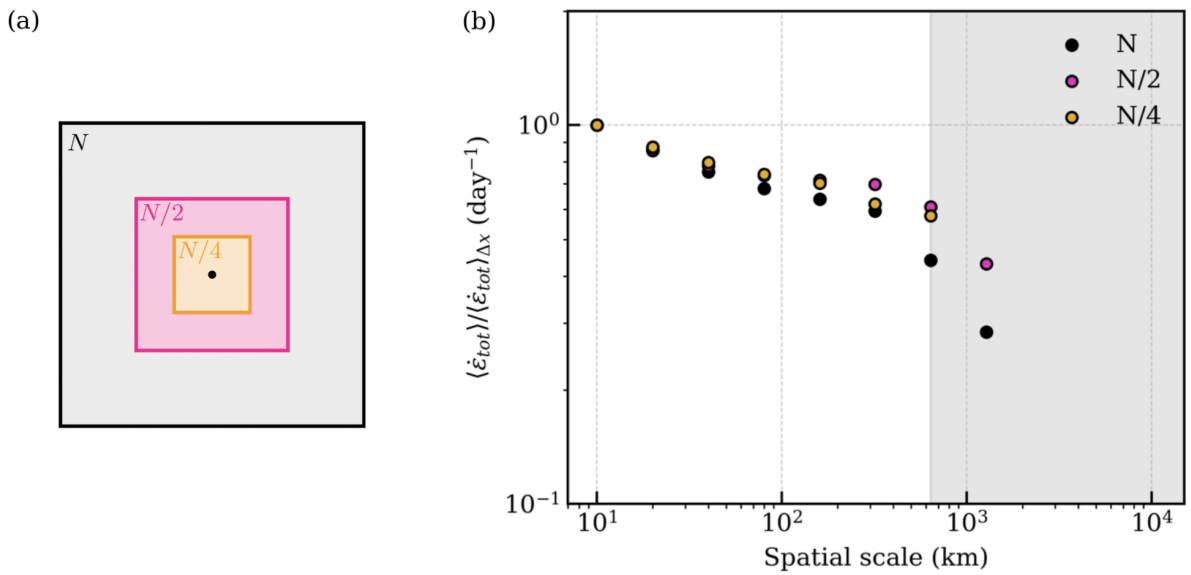


Figure R3: New Fig. 10

L.355-356: "These questions need to be addressed by developing targeted scale invariance diagnostics that are sensitive to non-stationarity, isotropy, and directional/tensorial information of the deformation fields" -> It is unclear if the authors already have an idea what kind of metrics this could be. If there are suggestions, please name them, if not please state that those still need to be identified.

We now state explicitly that these diagnostics remain to be identified (L355-356).

These questions need to be addressed by exploiting new high-resolution satellite datasets, which provide expanded spatial and temporal coverage in a changing Arctic sea ice system, and by developing targeted scale invariance diagnostics sensitive to non-stationarity,

isotropy, and the directional and tensorial properties of the deformation field. Such diagnostics remain to be identified.

References:

- Hutchings, J. K., Roberts, A., Geiger, C. A., & Richter-Menge, J. (2011). Spatial and temporal characterization of sea-ice deformation. Annals of Glaciology, 52(57), 360–368. https://doi.org/10.3189/172756411795931769

- Oikkonen, A., Haapala, J., Lensu, M., Karvonen, J., & Itkin, P. (2017). Small-scale sea ice deformation during N-ICE2015: From compact pack ice to marginal ice zone. Journal of Geophysical Research: Oceans, 122(6), 5105–5120. https://doi.org/10.1002/2016jc012387

- Hutchings, J. K., Bliss, A. C., Mondal, D., & Elosegui, P. (2024). Sea Ice Deformation Is Not Scale Invariant Over Length Scales Greater Than a Kilometer. Geophysical Research Letters, 51(12). https://doi.org/10.1029/2024gl108582

Additional references:

Girard L., Bouillon S., Weiss J., Amitrano D., Fichefet T., and Legat V. (2011). A new modeling framework for sea-ice mechanics based on elasto-brittle rheology. Annals of Glaciology, 52(57), 123–132. doi:10.3189/172756411795931499

Losch, M., Menemenlis, D., Campin, J.-M., Heimbach, P., and Hill, C.. On the formulation of sea-ice models. Part 1: Effects of different solver implementations and parameterizations. Ocean Modelling, 33(1), 129–144. https://doi.org/10.1016/j.ocemod.2009.12.008, 2010.

Vancoppenolle, M., Rousset, C., Blockley, E., Aksenov, Y., Feltham, D., Fichefet, T., Garric, G., Guémas, V., Iovino, D., Keeley, S., Madec, G., Massonnet, F., Ri- dley, J., Schroeder, D., and Tietsche, S.: SI3, the NEMO Sea Ice Engine (4.2release_doc1.0), Zenodo, https://doi.org/10.5281/zenodo.7534900, 2023.

Adcroft, A., Anderson, W., Balaji, V., Blanton, C., Bushuk, M., Dufour, C. O., Dunne, J. P., Griffies, S. M., Hallberg, R., Har- rison, M. J., Held, I. M., Jansen, M. F., John, J. G., Krasting, J. P., Langenhorst, A. R., Legg, S., Liang, Z., McHugh, C., Radhakrishnan, A., Reichl, B. G., Rosati, T., Samuels, B. L., Shao, A., Stouffer, R., Winton, M., Wittenberg, A. T., Xi- ang, B., Zadeh, N., and Zhang, R.: The GFDL Global Ocean and Sea Ice Model OM4.0: Model Description and Simu- lation Features, J. Adv. Model. Earth Sy., 11, 3167–3211,

https://doi.org/10.1029/2019MS001726, 2019.

Bouillon, S., Ángel Morales Maqueda, M., Legat, V., and Fichefet, T.: An elastic–viscous–plastic sea ice model formu- lated on Arakawa B and C grids, Ocean Model., 27, 174–184, https://doi.org/10.1016/j.ocemod.2009.01.004, 2009.

Lemieux, J.-F., Lipscomb, W. H., Craig, A., Bailey, D. A., Hunke, E. C., Blain, P., Rasmussen, T. A. S., Bentsen, M., Dupont, F., Hebert, D., and Allard, R.: CICE on a C-grid: new momentum, stress, and transport schemes for CICEv6.5, Geosci. Model Dev., 17, 6703–6724, https://doi.org/10.5194/gmd-17-6703-2024, 2024.